



The influence of perturbation motion over a slender delta wing under sideslip angle

Salınım hareketinin sapma açısı altındaki bir delta kanada etkileri

Mehmet Oğuz Taşcı¹ , Sergen Tümse¹ , Beşir Şahin^{1,*} , İlyas Karasu² , Hüseyin Akıllı¹ 

¹ Çukurova University, Faculty of Engineering, Department of Mechanical Engineering, Adana

² Adana Alparslan Türkeş Science and Technology University, Faculty of Aeronautics and Astronautics, Adana

Abstract

In this study, the main objective is to reveal the change of the vortical flow characteristics on a slender delta wing with a sweep angle of $A=70^\circ$ under the alteration of three different sideslip angles of $\beta=0^\circ$, 4° , and 8° at three different main angles of attack of $\alpha_m=25^\circ$, 30° and 35° experimentally. Dye visualization experiments were conducted at a Reynolds number of $Re=2 \times 10^4$ to analyze qualitatively. The perturbation motion which has amplitudes of $\alpha_0=\pm 0.5^\circ$ and $\pm 1^\circ$ was applied continuously under the periods of time of $T_c=0.5s$, $1s$, and $2s$. However, the effects of the low-frequency perturbations to which the aircraft is exposed during the maneuver were examined. It is observed that Kelvin-Helmholtz in the case of the perturbed motion vortices is more prominent than static case results of the slender delta wing. The vortex breakdown location on the perturbed delta wing has been changed in a wider range than the static case of the delta wing at zero sideslip angle, β .

Anahtar kelimeler: Angle of attack, Delta wing, Dye visualization, Perturbation motion, Sideslip angle

1 Introduction

Due to high lift and maneuver capacity, delta wings are usually employed on Unmanned Combat Aerial Vehicles (UCAVs), Unmanned Air Vehicles (UAVs), and Micro Air Vehicles and fighter jets. Munro et al. [1] expressed that delta wings are categorized as slender and non-slender depending on the sweep angle, A . They stated that if A is higher than or equal to 65° , it is named as slender otherwise, it is categorized as a non-slender delta wing. The vortex breakdown is one of the key parameters which is very influential on the aerodynamic performance and the structure of leading-edge vortices around the delta wing. Because the breakdown of the leading-edge vortices and unsteady flow structure disrupt the performance of the aircraft, so that reason the control of vortex breakdown is vital. Cui et al. [2] stated that the vortex breakdown has a profound impact on the aerodynamic forces of an aircraft. At the same time, the vortex breakdown causes the drag coefficient, C_D , to increase as it decreases lift coefficient, C_L . Vortex bursting can be identified as a quick dilatation of the structure of vortical flow and profound alteration of its velocity field and the existence of great-scale fluctuations as stated by Delery [3] and Payne et al. [4]. The phenomenon of vortex breakdown can be observed in three different types, namely bubble, spiral, and double helix type vortex breakdown. Figure 1 shows the various types of vortex breakdown. In the

Özet

Bu çalışmada, süpürme açısı $A=70^\circ$ olan narin (slender) delta kanadın girdaplı akış yapısındaki değişimi, sapma açısı $\beta=0^\circ$, 4° ve 8° karşısındaki değişimi, üç farklı ortalama hücum açısında $\alpha_m=25^\circ$, 30° ve 35° boya deneyi incelemesi amaçlanmıştır. Boya ile nitel görselleştirme deneyleri, $Re=2 \times 10^4$ gerçekleştirilmiştir. Kanat modeli istenilen açıda sabitlenerek ve elde edilen deney sonuçlar dikkate alınarak, $\alpha_0=\pm 0.5^\circ$ ve $\pm 1^\circ$ genişliğinde ve $T_c=0.5s$, $1s$ ve $2s$ periyotlarında kanata sürekli salınım hareketi verilerek girdap çökmesinin belirli ölçüde kontrolü sağlanmaya çalışılmıştır. Ancak, uçağın manevra sırasında maruz kaldığı düşük frekanslı bozulmaların etkileri incelenmiştir. Kelvin-Helmholtz girdaplarının narin delta kanadın daimi salınım hareketi verilen durumunda statik vaka sonuçlarından daha belirgin olduğu gözlenmektedir. Narin delta kanatlarının sıfır sapma açısı, β salınımı hareketi anında; girdap çökme konumu statik durumdan daha geniş bir aralıkta ileri ve geri hareket etmektedir.

Keywords: Boya ile görselleştirme, Delta kanat, Hücum açısı, Salınım hareketi, Sapma açısı.

investigation of Gursul et al. [5], it was expressed that the structure of the vortical flow of a delta wing is made up of two counter-rotating leading-edge vortices. Moreover, they resulted that separated flow from leading edge forms a curved free shear layer rolling up into a core. Vortex meandering can be attributed to the non-linear interaction of small-scale vortices produced by Kelvin-Helmholtz instability and neighboring large-scale vortices (primary vortex). Jaquin et al. [6] offered different physical reasons for vortex meandering; nonstable leading-edge vortices caused by unsteadiness of test facility, the turbulence in the neighboring shear layer; non-linear interactions of various instability mechanisms; and progression of unsteadiness from the test model. Beresh et al. [7] stated that the turbulence arising at the test facility wall contributes to the vortex meandering by energizing the incoming boundary layer. For further information about vortex meandering, refer to [8-10]. The vortex breakdown and its effect on the performance of aerodynamic systems and flow characteristics on the wing were studied by several authors [11-17]. The flow over a slender delta wing demonstrates a profound viscous effect at low Reynolds numbers, $Re=10^3$ - 10^4 . Further increase of Reynolds number more than $Re=10^4$, the impact of viscosity is decreased and at the Reynolds number, $Re=2 \times 10^4$, the profound viscous effect is attenuated, and the flow reaches the asymptotic state. Further increase of the Reynolds number induces just small variations on the

* Sorumlu yazar / Corresponding author, e-posta / e-mail: bsahin@cu.edu.tr (B. Şahin)

Geliş / Received: 15.08.2020 Kabul / Accepted: 22.12.2020 Yayınlanma / Published: 15.01.2021

doi: 10.28948/ngumuh.780989

flow structure of the delta wing. Erickson [18] expressed that the flow characteristics on a slender delta wing is not dependent on the Reynolds number for $Re > 10^4$ at high angles of attack. Gursul [19] revealed that high-velocity fluctuations in the vortex core are not dependent on the Reynolds number and model geometry.

The breakdown of leading-edge vortices and transient flow structure can be suppressed by different flow control methods. Gursul et al. [20] revealed that different flow control techniques could be employed to the delta wings to postpone the breakdown of leading-edge vortices and reattach the separated flow to the delta wing surface. In the study of Shen et al. [21], the asymmetrical aerodynamic structure of a 75° swept delta wing was tried to control by the plasma method at the Reynolds number, $Re = 5 \times 10^4$. They stated that an earlier vortex breakdown happened in the region where the plasma control technique was applied while the breakdown of leading-edge vortices was suppressed in the zone free from the method of plasma control. In the study of Hadidoolabi and Ansarian [22], the flow structure around 60° swept delta wing having sharp leading edges exposed to pitching maneuver at a variety of starting and final angles was computationally investigated from subsonic to supersonic flow regimes. They found that the chordwise location of leading-edge vortex bursting moved upstream and following the termination of maneuver. The impact of the rotating propeller on the vortical flow structure of the delta-winged unmanned aerial vehicle with sharp leading edges was studied by Zain et al. [23]. The results demonstrated that a rotating propeller on the model augments the aerodynamic efficiency of the delta-winged

unmanned aerial vehicle. The other result that can be inferred from this study is that the rotating propeller retards the vortex breakdown. It is vital in applications to have knowledge about the aerodynamic properties of the delta wing in unstable motion. The nature of the breakdown structure and the advance of the separated flow region on the surface of the slender delta wing having $\Lambda = 75^\circ$ at higher angles of attack such as $\alpha = 24^\circ, 30^\circ, 32^\circ$, and 35° were examined by Ozgoren et al. [24]. As a conclusion of their results, it is showed that the size of the downstream of the vortical flow over the slender delta wing increased to a higher level by the enhancement of the angle of attack, α . Also, the region of turbulent flow was widened, and turbulent fluctuation levels increased rapidly. Buzica et al. [25] experimentally worked on active flow control by using pulsed blowing on a slender delta wing having a sweep angle of $\Lambda = 65^\circ$ at high angles of attack such as $\alpha = 23^\circ, 35^\circ$ and 45° . The high aspect ratio slots were placed along the leading edges of the slender delta wing to blow percussively. In this study, the angles of attack, α are adjusted in three different zones: pre-stall zone, stall zone, and post-stall zone. The aerodynamic coefficients increase with the angle of attack, α up to the pre-stall zone. However, as the angle of attack, α increases further, the aerodynamic coefficients begin to decrease. Cetin et al. [26] expressed that the active flow control technique with periodic blowing along the leading edge of the wing is very effective in preventing the regional separation over the surface of the wing. The steady blowing through the leading edge of the wing changed the flow characteristics substantially and this blowing is very influential to diminish three-dimensional flow separation as indicated in the study of Zharfa et al [27].

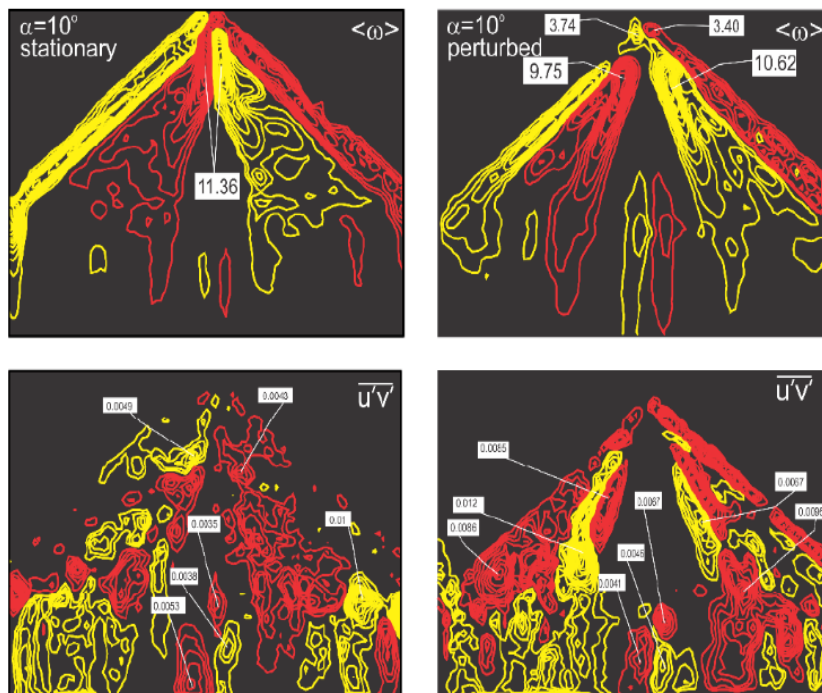


Figure 1. The patterns of time-averaged vorticity and transverse velocity components for the delta wing under perturbed and static conditions at a mean angle of attack, $\alpha_m = 10^\circ$ [28].

Canpolat et al. [28] studied the turbulence statistics experimentally, and the structure of leading-edge vortices over 40° swept diamond and delta wings. The wings were exposed to perturbation with the amplitude of $\alpha_0 = \pm 0.5^\circ$ and oscillation period of $T_e = 0.5s$. The dye visualization and quantitative observation using the stereo particle image velocimetry (SPIV) were conducted to inquire flow structure for α_m within the range of $7^\circ \leq \alpha_m \leq 17^\circ$. Fig. 1 demonstrates the structures of time-averaged vorticity and transverse velocity components for the delta wing under perturbed and static conditions at $\alpha_m = 10^\circ$.

In the investigation of Ozgoren [29], the change of the structure of leading-edge vortex and vortex breakdown on a delta wing under the sinusoidally pitching motion was investigated experimentally. He reported that the structure of the vortex core and the vortex breakdown region depends on the amplitude of the angle of attack, α . Also, the impact of reduced frequency, K and time lag on the structure of vortical flow was studied. Yaniktepe and Rockwell [30] revealed that when the wing is perturbed with a small amplitude, the magnitude and distributions of instantaneous and time-averaged flow structure alters significantly. The dynamic behavior of leading-edge vortices over a pitching delta wing which has a 70° sweep angle, Λ was researched by LeMay et al. [31]. They reported that when the delta wing is sinusoidally pitched, the hysteresis is observed. This hysteresis rises with increasing reduced frequency, K . A

delta wing with a sweep angle of $\Lambda = 30^\circ$ was perturbed at a constant pitch rate from 0° to 60° to investigate the impact of perturbed motion on the flow characteristics in the research of Gilliam et al. [32]. He found that the consistency and size of leading-edge vortices rise with increasing pitch rate. Moreover, it was noted that the location of the vortex breakdown does not change during the period of starting the pitching motion. In the work of Reynolds and Abtahi [33], a delta wing was pitched at a constant rate of $K = 0.06$ for angles of attack within the range of $30^\circ \leq \alpha \leq 51^\circ$ at Reynolds numbers, $Re = 19 \times 10^3$ and 65×10^3 . They stated that large time delays are detected related to the vortex breakdown position comparing to the static case, and hysteresis was observed in the response of the vortex flow between the pitching-up and pitching-down cases. Gursul and Wang [34] conducted an experimental work over a 75° swept delta wing to search the vortex breakdown core. It was reported that the root means square (RMS) values at the origin of the vortex breakdown decrease at the lower Reynolds number, Re . Because the shear layer does not exhibit the instability of Kelvin-Helmholtz (K-H), but it is observed that after a critical Reynolds number, Re , the shear layer is dominated by a vortical flow structure because of the instability of Kelvin-Helmholtz (K-H). LeMay et al. [35] examined the dynamic characteristics of the leading-edge vortices over a pitching delta wing which has a 70° sweep angle, Λ .

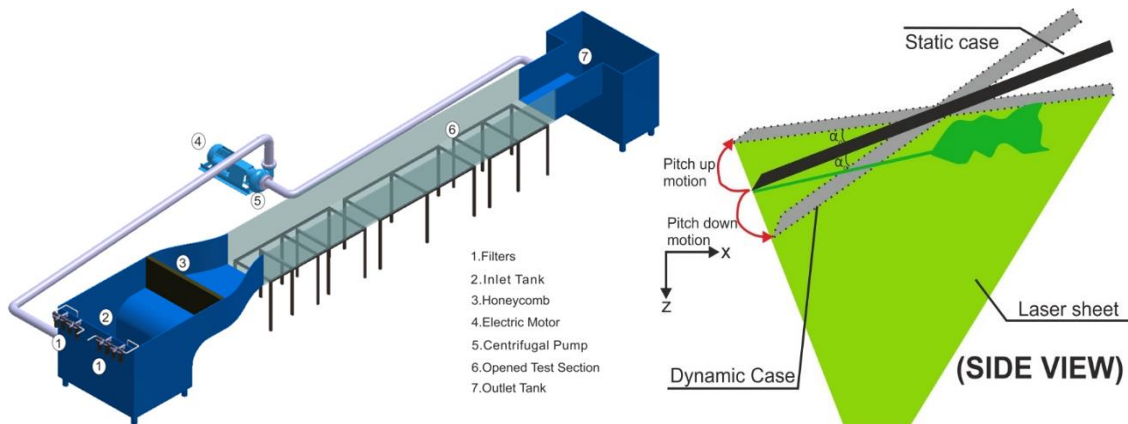


Figure 2. The schematic representation of the water channel and the perturbation motion of the delta wing.

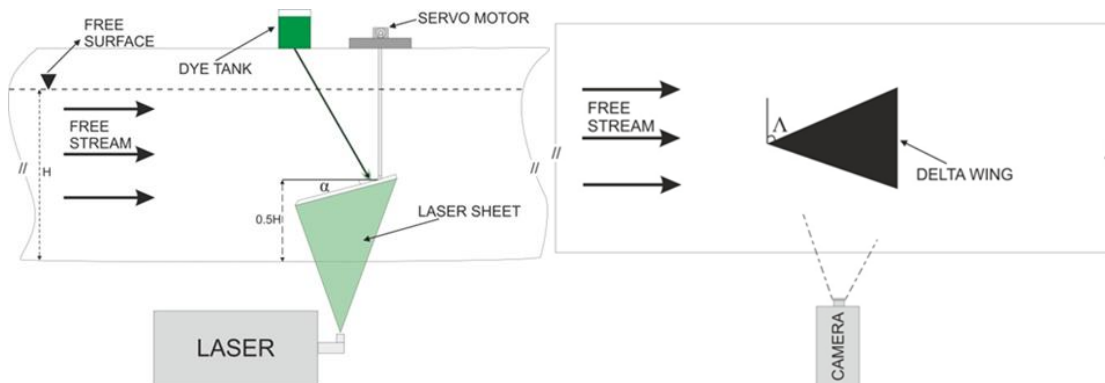


Figure 3. The schematic representation of the setup of the perturbation motion.

The reduced frequency, K is defined as $2\pi fC/U_{ref}$ where f is the oscillation frequency, C is the chord of the delta wing, U_{ref} is the free-stream velocity. When the delta wing was sinusoidally pitched, the hysteresis is observed [35]. This hysteresis increases with increasing the reduced frequency, K . Grismer and Nelson [36] investigated the impact of the oscillating motion on the aerodynamic behavior of double delta wing under the sideslip angle, β . They emphasized that the discrepancy of the vortex breakdown positions between upstroke and downstroke pitching motion of the delta wing can be altered further by increasing K . In the survey of Ozgoren and Sahin [37], the delta wing was pitched for three different value of angles of attack, $\alpha=20^\circ$, 24° , and 30° at an amplitude of perturbation $\alpha_0=10^\circ$ at a lower frequency. It was observed that the vortex breakdown, leading-edge vortices, and separation region substantially influenced during the pitching motion of the delta wing, and the structure of vortical flow alters as a function of oscillations.

The purpose of this investigation is to reveal the impact of perturbation of the delta wing on the vortex bursting location and vortical flow characteristics by employing dye visualization technique under sideslip angle, β . Also, the interaction between leading-edge vortices and delta wing surfaces after the vortex breakdown was studied. The studies from the literature that commonly expose the impact of the sideslip angle, β on the aerodynamics of the non-slender delta wings. The aim of the current study aims to provide comprehensive information about the physics of flow on the slender delta wing with the sweep angle of $\Lambda=70^\circ$ in the side-view plane. Particularly, considering the variations of sideslip angle, β and the perturbation motion, there is not enough research work providing information about the aerodynamics of slender delta wing with $\Lambda=70^\circ$ in the side-view plane under the variations of α , β and T_e using the dye

visualization technique. In this study, it is also aimed to examine how the low amplitude movement behaves along the delta wing surface and its effects on the leading-edge vortices and the interactions during the maneuver of the delta wing affected by the variations of α , β and T_e . The ability of the delta wing is impaired under the variation of α , β and T_e . The point that distinguishes this study from previous studies is to analyze the variation of the aerodynamic features on the slender delta wing with $\Lambda=70^\circ$ visualizing sets of instantaneous images to reveal the physics of flow in detail, qualitatively.

2 Material and method

Experiments were performed in a closed-loop free surface water tunnel with dimensions of 8 m length, 1 m width and 0.75 m height. The water channel consists of Plexiglas material having a thickness of 15 mm. There are two water tanks on this channel; one of them is positioned at the entrance, and the other one is placed at the outlet of the water tunnel. There is a contraction section of 2:1 ratio to ensure the passage between the water tank at the inlet and test section of the water channel. A honeycomb located before the contraction section of 2:1 ratio is used to regulate upstream flow and turbulence intensity. There are small cylindrical pipes in the honeycomb which prevent fluctuations in the water. The particular design of the water tunnel and the use of the flow regulator provide the turbulence intensity to be kept below 0.4 %. The speed and circulation of the water in the channel are adjusted by a centrifugal pump with a 15kW power capacity which can operate at different speeds with the help of a frequency control unit. The water tunnel is schematically displayed in Figure 2.

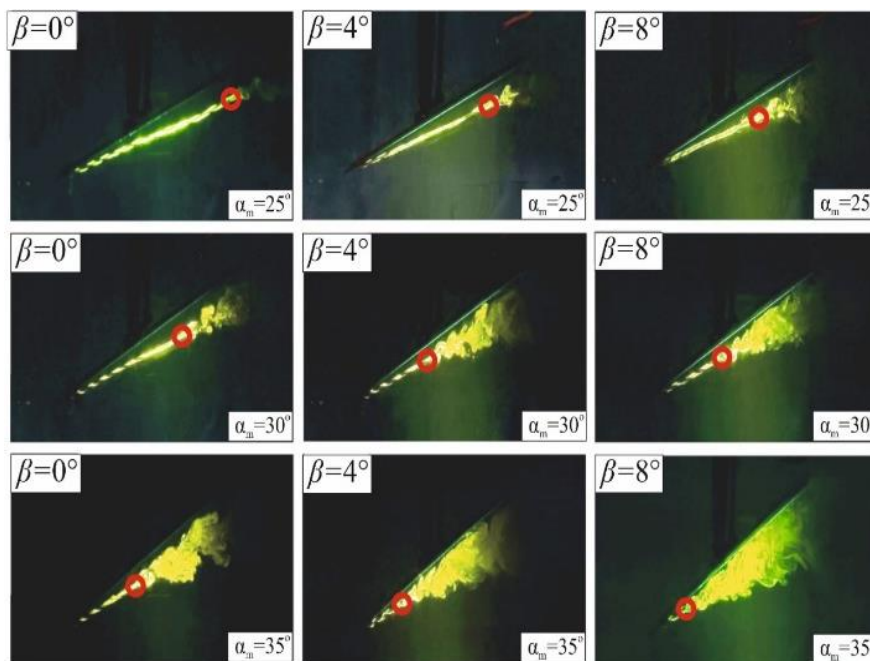


Figure 4. The representation of dye visualization experiments for the static case under the alteration of three different sideslip angles of $\beta=0^\circ$, 4° , and 8° at the main angle of attack of $\alpha_m=25^\circ$, 30° , and 35° .

The dye flow visualization technic is known as the way which presents prior or qualitative knowledge about the vortical flow structure formed on the delta wing. In dye flow visualization experiments, a Rhodamine 6G type fluorescent dye that shines under the laser light having 532 nm wavelengths was utilized to detect the leading-edge vortices around the delta wing. This fluorescent dye was mixed with water before the experiment. The dye was injected over the delta wing from the tank placed at a certain height with the help of a thin hose. The needle at the end of this hose was located in the channel formed through the central axis of the delta wing. The dye reached the tip of the delta wing by moving along this channel. A Sony HD-SR1 camera was employed to capture images acquired during the experiments. The experimental setup of the dye flow visualization is schematically demonstrated in Figure 3. In the present study, the 70° swept delta wing with a 25 cm chord length, C was used and located in the middle of the flow.

3 Results and discussion

The images of dye visualization experiments, having a low amplitude of $\alpha_0 = \pm 0.5^\circ$ and $\pm 1^\circ$ and perturbation periods of $T_e = 0.5s, 1s, \text{ and } 2s$ at a Reynolds number of $Re = 2 \times 10^4$, of a highly swept ($\Lambda = 70^\circ$) slender delta wing under the change of three different yaw angles of $\beta = 0^\circ, 4^\circ, \text{ and } 8^\circ$ at three different main angles of attack of $\alpha_m = 25^\circ, 30^\circ, \text{ and } 35^\circ$, are shown in Figure 5 to Figure 10. In the dye visualization experiments, it was attempted to investigate the effects of perturbation motion on the breakdown of the leading-edge vortices at low amplitude, α_0 and low perturbation periods, T_e . The dye visualization experiments were carefully watched and it was seen that the locations of the vortex breakdown of the leading-edge vortices sometimes moved

towards the tip of the delta wing and sometimes towards the trailing edge of the delta wing and this vortical flow motion has no periodic structure. A similar motion of the vortex breakdown was also detected in the static case of the delta wing. However, the breakdown position of the leading-edge vortex on the perturbed delta wing has been changed in a wider range than the static case of the delta wing at $\beta = 0^\circ$. After watching the dye video recordings carefully, it was observed that the vortex breakdown period was approximately 0.5s, and the period time of the perturbation motion was accordingly determined as $T_e = 0.5s, 1s, \text{ and } 2s$. In addition, perturbing the slender delta wing with the frequency which was taken more than an order of magnitude higher or lower than the inherent frequency of vortex breakdown in discrete mode was aimed to see the impact of perturbation motion. The dye video recordings are long enough to observe the development of the natural vortex structure, and they are in the range, approximately 5-10 minutes.

Considering the dye visualization results obtained by the given yaw angles, β and main angles of attack, α_m for the edge of the delta wing, exposed to the wind, having the amplitude of $\alpha_0 = \pm 0.5^\circ$ and $\pm 1^\circ$ and the perturbation periods of $T_e = 0.5s, 1s \text{ and } 2s$ or the frequency which was taken more than an order of magnitude higher or lower than the inherent frequency of vortex breakdown or equal to the inherent frequency, it was tried to see the possibility of controlling the location of the onset of the vortex breakdown of the slender delta wing. Low perturbation periods, T_e and perturbation amplitudes, α_0 were used to determine the vortex breakdown points of leading-edge vortices by dye visualization experiments and to compare with static case results as shown in Figure 4.

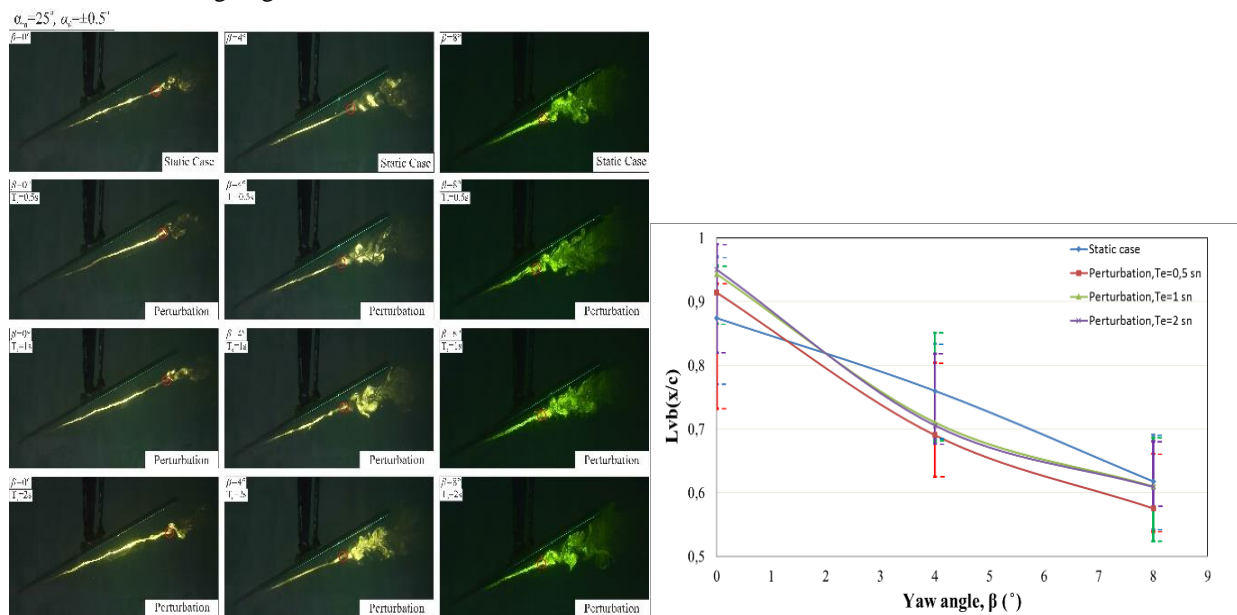


Figure 5. The presentation of dye visualization experiments, having low amplitude ($\alpha_0 = \pm 0.5^\circ$) and perturbation periods ($T_e = 0.5s, 1s, \text{ and } 2s$) under the alteration of three different yaw angles of $\beta = 0^\circ, 4^\circ, \text{ and } 8^\circ$ at three different main angles of attack of $\alpha_m = 25^\circ$ and the effect of low amplitude perturbation conditions on the mean vortex breakdown locations, x/C .

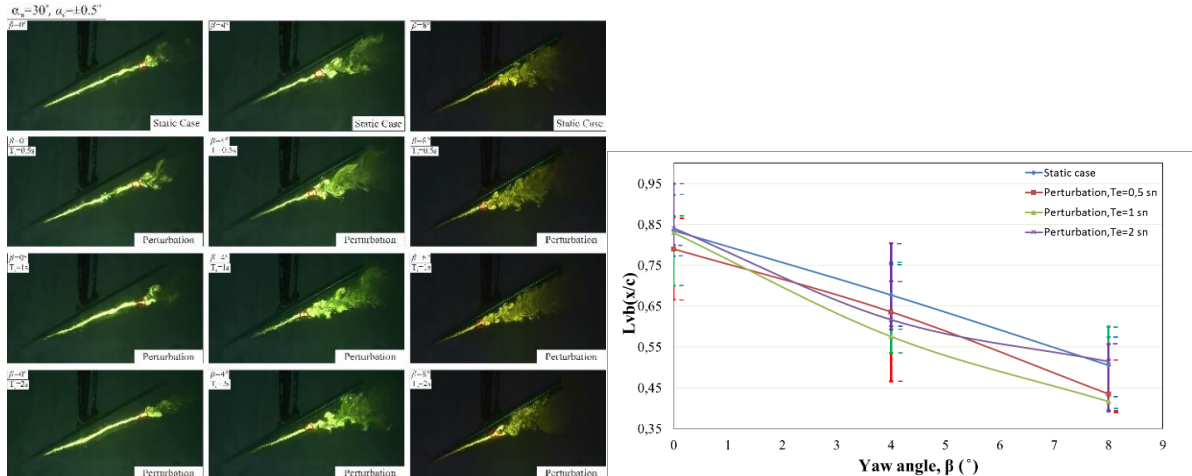


Figure 6. The presentation of dye visualization experiments, having low amplitude ($\alpha_0=\pm 0.5^\circ$) and perturbation periods ($T_e=0.5s, 1s,$ and $2s$) under the alteration of three different yaw angles of $\beta=0^\circ, 4^\circ,$ and 8° at three different main angles of attack of $\alpha_m=30^\circ$ and the effect of low amplitude perturbation conditions on the mean vortex breakdown locations, x/C .

The permanent sinusoidal perturbation motion given to the delta wing is defined by the expression of $\alpha(t)=\alpha_m+\alpha_0\sin\omega_e t$ where the angular velocity is $\omega_e=2\pi f_e$, α_m is the mean angle of attack, α_0 is the amplitude of the perturbation, and $t=T_e$ is the period of perturbation motion. The effect of low amplitude perturbation conditions on the average vortex breakdown locations was interpreted. The vortex breakdown location, x/C was numerically given in Figures 5-7. In the first line of dye visualization images, the delta wing was kept constant at different angles of attack, α_m . In the other three lines of the figures, the change of vortex breakdown location of the leading-edge vortices under perturbation motion was given. The circle indicated by the red color in the dye visualization images shows the vortex breakdown location of the leading-edge vortices. The graph

just below the images shows how the vortex breakdown point behaves against the perturbation motion according to the yaw angle, β for each case of the experiments.

As shown in Figure 5, the mean attack angle of the delta wing is taken as $\alpha_m=25^\circ$. And, the angular amplitude of the perturbation motion was taken as $\alpha_0=0.5^\circ$. The period of wing perturbation was applied as $T_e=0.5s, 1s,$ and $2s$. Low periods of perturbation time, T_e and amplitude of the perturbation motion, α_0 were used to determine the collapse points of wingtip vortices by dye experiments compared with static delta wing results. As shown in the figure, when the perturbation motion is given to the delta wing at zero yaw angle, β , the vortex breakdown location was moved from $x/C=0.87$ to $x/C=0.95$ in the periods of time of $T_e=1s$ and $2s$.

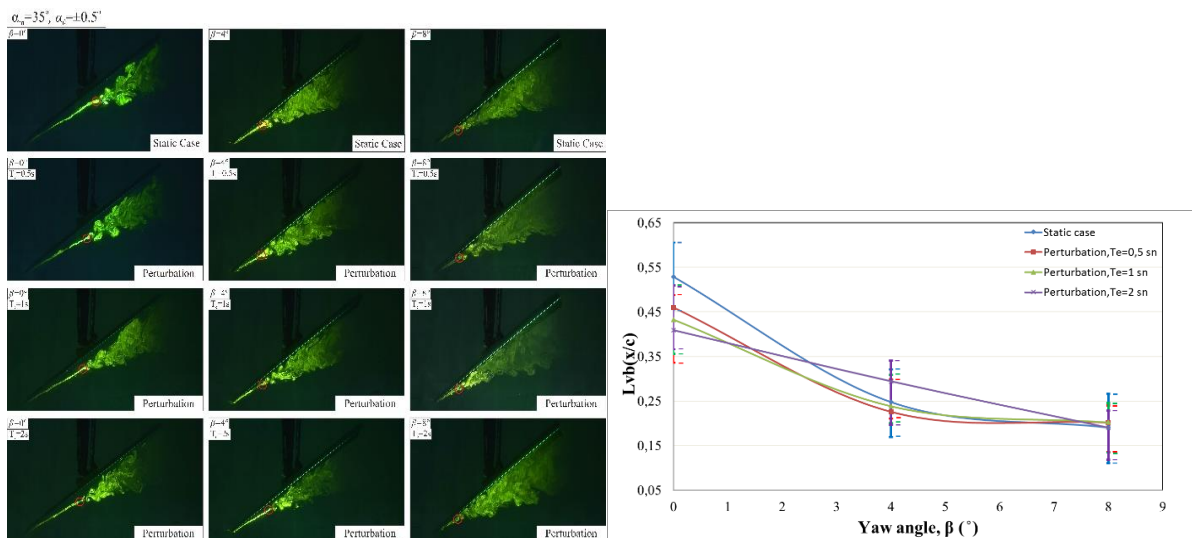


Figure 7. The presentation of dye visualization experiments, having low amplitude ($\alpha_0=\pm 0.5^\circ$) and perturbation periods ($T_e=0.5s, 1s,$ and $2s$) under the alteration of three different yaw angles of $\beta=0^\circ, 4^\circ,$ and 8° at three different main angles of attack of $\alpha_m=35^\circ$ and the effect of low amplitude perturbation conditions on the mean vortex breakdown locations, x/C .

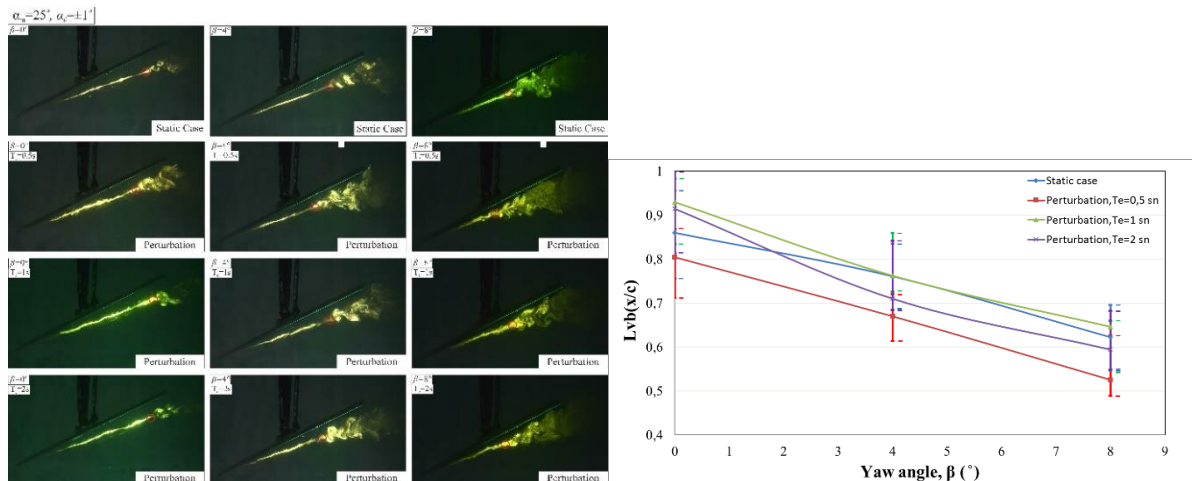


Figure 8. The representation of dye visualization experiments, having low amplitude ($\alpha_0=\pm 1^\circ$) and perturbation period ($T_e=0.5s, 1s, \text{ and } 2s$) under the alteration of three different sideslip angles of $\beta=0^\circ, 4^\circ, \text{ and } 8^\circ$ at three different main angles of attack of $\alpha_m=25^\circ$ and the effect of low amplitude perturbation conditions on the mean vortex breakdown locations, x/C .

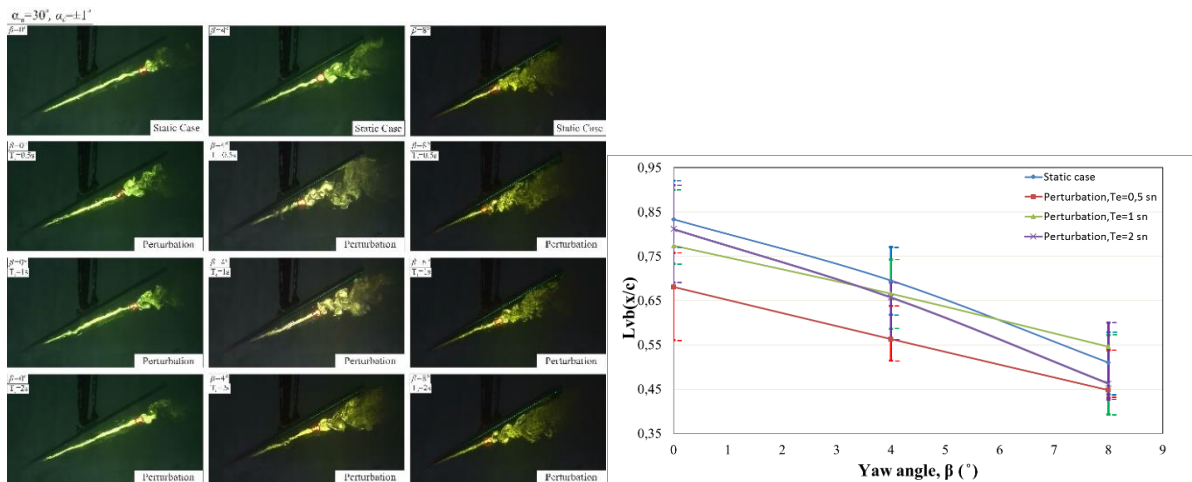


Figure 9. The representation of dye visualization experiments, having low amplitude ($\alpha_0=\pm 1^\circ$) and perturbation period ($T_e=0.5s, 1s, \text{ and } 2s$) under the alteration of three different sideslip angles of $\beta=0^\circ, 4^\circ, \text{ and } 8^\circ$ at three different main angles of attack of $\alpha_m=30^\circ$ and the effect of low amplitude perturbation conditions on the mean vortex breakdown locations, x/C .

As known, water is an incompressible fluid. While the delta wing is in perturbation motion, the delta wing operates pushing the water in the direction of flow even though it is a very short distance. This movement gives the water some energy. In other words, there is an increase in the kinetic energy of water. On the other hand, there is a slight reduction in the kinetic energy of the leading-edge vortices, moving in the direction of free stream flow, creating a slight volumetric gap on the trailing edge of the delta wing. It is thought that this will not affect the vortex breakdown point in the opposite direction as the perturbation time, T_e is very short. However, when the β is set to 4° , the vortex breakdown position is moved from $x/C=0.76$ to 0.70 . When β is shifted to 8° , it is seen that the vortex breakdown point is moved forward compared to the static case of the delta wing.

As shown in Figure 6, the mean angle of attack, α , and amplitude of the perturbation motion were taken as $\alpha_m=30^\circ$ and $\alpha_0=\pm 0.5^\circ$, respectively. The period of wing perturbation was changed as $T_e=0.5s, 1s, \text{ and } 2s$. One of the important parameters in determining the perturbation periods, T_e is that the natural frequency of the vortices occurring at the vortex breakdown point of the leading-edge vortices is around $0.5s$ on average. Therefore, the determined period values of perturbation motion were multiples of the natural frequency of the vortices. In general, when the mean angle of attack of the delta wing, α_m is increased to 30° , the vortex breakdown point approaches the tip of the delta wing. As explained extensively in the previous dye experiments, the vortex breakdown locations, x/C approach tip of the delta wing at all three periodic values of perturbation motion.

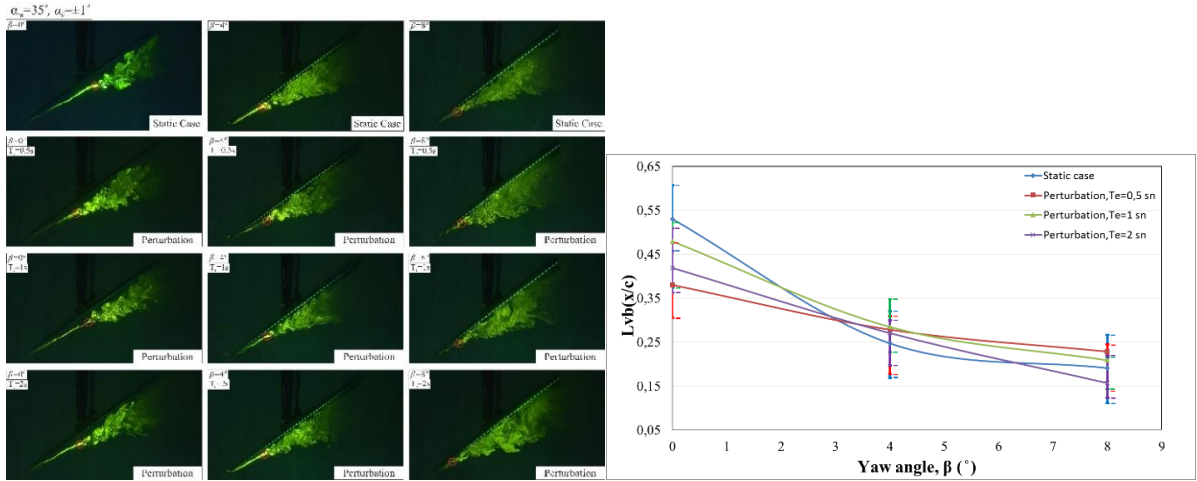


Figure 10. The representation of dye visualization experiments, having low amplitude ($\alpha_0=\pm 1^\circ$) and perturbation period ($T_e=0.5s, 1s,$ and $2s$) under the alteration of three different sideslip angles of $\beta=0^\circ, 4^\circ,$ and 8° at three different main angles of attack of $\alpha_m=35^\circ$ and the effect of low amplitude perturbation conditions on the mean vortex breakdown locations, x/C .

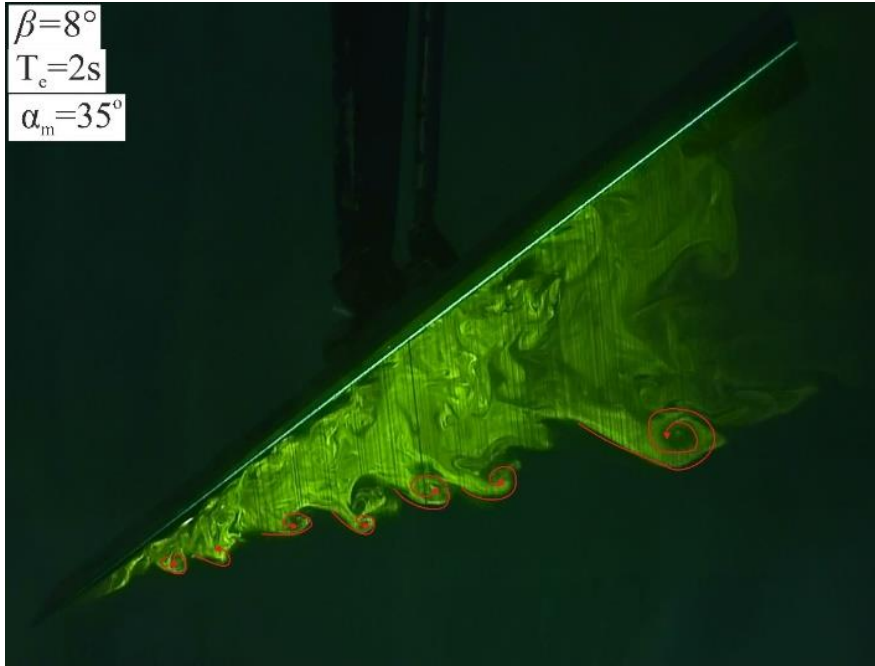


Figure 11. The presentation of the clear vision of the Kelvin-Helmholtz vortices over the delta wing.

As seen in Figure 7, the mean angle of attack, α , and amplitude of the perturbation motion were taken as $\alpha_m=35^\circ$ and $\alpha_0=\pm 0.5^\circ$, respectively. The period of delta wing perturbation was changed as $T_e=0.5s, 1s$ and $2s$. In the case of yaw angle of $\beta=4^\circ$ and perturbation period, $T_e = 2s$, the vortex breakdown location, x/C moves towards the trailing edge of the delta wing, and in the case of yaw angle of $\beta=0^\circ$, the perturbation movements involving all periods, T_e carried the vortex breakdown location, x/c to the tip of the delta wing. When the yaw angle, β is 8° , the perturbation effect is almost negligible compared to the static case.

As shown in Figure 8, the average angle of attack, α , and amplitude of the perturbation motion were taken as $\alpha_m=25^\circ$ and $\alpha_0=\pm 1^\circ$, respectively. The period of wing perturbation

was changed as $T_e=0.5s, 1s$ and $2s$. One of the critical parameters in determining the perturbation periods, T_e is that the natural frequency of the vortices occurring at the vortex breakdown point of the leading-edge vortices is around $0.5s$ on average. Therefore, the determined period values of perturbation motion were multiples of the natural frequency of the vortices.

Also, in Figure 9, when the perturbation motion is given to the delta wing at zero sideslip angle, β , the vortex breakdown point was moved from $x/C=0.86$ to 0.92 in $T_e=1s$ and $2s$ periods. However, the vortex breakdown point was partially moved towards the tip of the delta wing at the period of perturbation motion of $T_e=0.5s$.

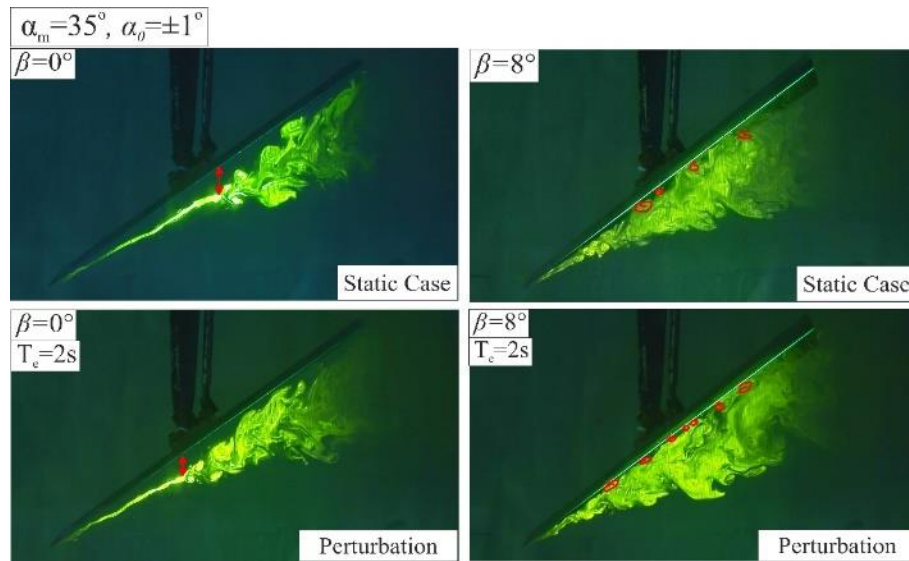


Figure 12. The presentation of the interaction between leading-edge vortices and delta wing surface.

It was seen that the experimental results give different results in the perturbation motions at different periods. In general, the vortex breakdown point is arbitrary in the direction of free flow or vice versa. In other cases (the perturbed delta wing) the vortex breakdown point also is not constant.

The average angle of attack, α and amplitude of the perturbation motion were taken as $\alpha_m=35^\circ$ and $\alpha_0=\pm 1^\circ$, respectively as shown in Figure 10. The period of wing perturbation was changed in the range of $T_e=0.5s$, $1s$, and $2s$, similarly. It was observed that the vortex breakdown point was moved further to the tip of the delta wing at the double value of the natural frequency of the perturbation motion. As shown in Figure 4, the average angle of attack, α , and amplitude of the perturbation motion were taken as $\alpha_m=35^\circ$ and $\alpha_0=\pm 1^\circ$, respectively. The period of wing perturbation was changed in the range of $T_e=0.5s$, $1s$, and $2s$, similarly. The difference between the experiments of static and perturbation motion decreases as the sideslip angle, β increases.

As shown in Figure 11, Kelvin-Helmholtz vortices become more pronounced with the increment of the sideslip angle, β . The perturbation motion also plays an important role in the clarification of these vortices. As a result of the low amplitude perturbation motion, the delta wing is exposed to unsteady loading. When the unsteady loading exceeds a certain value, the buffeting occurs. The perturbation motion, which causes vibration, also allows the Kelvin-Helmholtz vortices to be seen more clearly from the side-view plane of the delta wing.

The interaction between leading-edge vortices and delta wing surfaces after the vortex breakdown was also observed. Before referring to the control of the vortex flow with perturbation motion, it is evidence that the increase in sideslip angle, β causes the leading-edge vortices to approach the surface of the delta wing as shown in Figure 12. In addition, the interaction between the surface of the delta wing and the flow structure increases when the perturbation motion under the sideslip angle, β increases. The vibration

movement having a small amplitude, α_0 applied to the delta wing causes the increase of the unsteady loads. Since the buffeting occurs according to the high intensity of the vibrations, the maneuverability is reduced.

4 Conclusion

The images of dye visualization experiments of a $A=70^\circ$ swept delta wing under the alteration of three different sideslip angles of $\beta=0^\circ$, 4° , and 8° at three different main angles of attack of $\alpha_m=25^\circ$, 30° , and 35° were performed at a Reynolds number of $Re=2 \times 10^4$ to analyze qualitatively. The perturbation motion which has amplitudes of $\alpha_0=\pm 0.5^\circ$ and $\pm 1^\circ$ was applied continuously under the periods of time of $T_e=0.5s$, $1s$, and $2s$ or the frequency which was taken more

than an order of magnitude higher or lower than the inherent frequency of vortex breakdown or equal to the inherent frequency in order to see the possibility of controlling the location of the onset of the vortex breakdown of the slender delta wing. In addition, perturbing the slender delta wing with the frequency which was taken more than an order of magnitude higher or lower than the inherent frequency of vortex breakdown in discrete mode was aimed to see the impact of perturbation motion. In this research, it is seen that the low perturbation period, T_e and small amplitude, α_0 values did not cause significantly large differences compared to the static case. It is estimated that the numerical values of the leading-edge vortices generated by perturbation motion may be greater. It is observed that Kelvin-Helmholtz vortices are more prominent than the static case results of the slender delta wing. The breakdown position of the leading-edge vortex, x/C on the perturbed delta wing, has been changed in a wider range than the static case of the delta wing at zero sideslip angle, $\beta=0^\circ$. It was also observed that the locations of the vortex breakdown of the leading-edge vortices, x/C sometimes moved towards the tip of the delta wing and sometimes towards the trailing edge of the delta wing, and this vortical flow motion has no periodic structure. A similar vortex breakdown motion was observed in the static case of the delta wing. In addition, the interaction

between leading-edge vortices and delta wing surfaces after the vortex breakdown was also observed. The interaction between the surface of the delta wing and the flow structure increases when the perturbation motion under the sideslip angle, β increases. Since the buffeting occurs according to the high intensity of the perturbation motion, the maneuverability of the delta wing is restricted.

Acknowledgement

The research described in this paper was financially supported by the Scientific and Technological Research Council of Turkey under contract no: 114M497. Additional financial support was also received from the Scientific Research Project Office of Çukurova University under contract no: FDK-2019-11368.

Conflict of interest

The authors declare that there is no conflict of interest.

Similarity rate (iThenticate): %14

References

- [1] C. Munro, P. Krus, and C. Jouannet, Implications of scale effect for the prediction of high angle of attack aerodynamics. *Progress in Aerospace Sciences*, 41 (3-4), 301–22, 2005. <https://doi.org/10.1016/j.paerosci.2005.05.001>
- [2] Y. D. Cui, T. T. Lim, and H. M. Tsai, Control of Vortex Breakdown over a Delta Wing Using Forebody Spanwise Slot Blowing. *AIAA Journal*, 45 (1), 110–117, 2007. <https://doi.org/10.2514/1.22575>
- [3] J. M. Delery, Aspects of vortex breakdown. *Progress in Aerospace Sciences*, 30 (1), 1–59, 1994. [https://doi.org/10.1016/0376-0421\(94\)90002-7](https://doi.org/10.1016/0376-0421(94)90002-7)
- [4] F. M. Payne, and R.C. Nelson, An experimental investigation of vortex breakdown on a delta wing. NASA Technical Report, N86-27196, 1986.
- [5] I. Gursul, Z. Wang, and E. Vardaki, Review of flow control mechanisms of leading-edge vortices. *Progress in Aerospace Sciences*, 43 (7-8), 246–70, 2007. <https://doi.org/10.1016/j.paerosci.2007.08.001>
- [6] Jaquin, J., Fabre, D., Geffroy, P., and Coustols, E., The Properties of a Transport Aircraft Wake in Extended Near Field: An Experimental Study. 39th Aerospace Sciences Meeting and Exhibit, AIAA Paper 2001-1038, USA 2001. <https://doi.org/10.2514/6.2001-1038>
- [7] S. J. Beresh, J. H. Henfling, and R. W. Spillers, Meander of a fin trailing vortex and the origin of its turbulence. *Experiments in Fluids*, 49 (3), 599–611, 2010. <https://doi.org/10.1007/s00348-010-0825-0>
- [8] G. V. Iungo, Wandering of a wing-tip vortex: rapid scanning and correction of fixed-point measurements. *Journal of Aircraft*, 54, 1-12, 2017. <https://doi.org/10.2514/1.C034120>
- [9] I. Gursul, and W. S. Xie, Origin of vortex wandering over delta wings. *Journal of Aircraft*, 37 (2), 348–50, 2000. <https://doi.org/10.2514/2.2603>
- [10] A. L. Heyes, R. F. Jones, and D. A. Smith, Wandering of wing-tip vortices. *Proceedings of the 12th International Symposium of Applied Laser Technologies for Fluid Mechanics*, Lisbon, 2004.
- [11] I. Gursul, M. Allan, and K. Badcock, Opportunities for the integrated use of measurements and computations for the understanding of delta wing aerodynamics. *Aerospace Science and Technology*, 9 (3), 181–189, 2005. <https://doi.org/10.1016/j.ast.2004.08.007>
- [12] I. Heron and R. Myose, On the impingement of von karman vortex street on a delta wing. 22nd Applied Aerodynamics Conference and Exhibit, Rhode Island USA, 16-19 August 2004. <https://doi.org/10.2514/1.12808>
- [13] B. Sahin, H. Akilli, J.-C. Lin, and D. Rockwell, Vortex Breakdown-Edge interaction: Consequence of edge oscillations. *AIAA Journal*, 39, 865–76, 2001. <https://doi.org/10.2514/2.1390>
- [14] R. C. Nelson and A. Pelletier, The unsteady aerodynamics of slender wings and aircraft undergoing large amplitude maneuvers. *Progress in Aerospace Sciences*, 39 (2-3), 185–248, 2003. [https://doi.org/10.1016/S0376-0421\(02\)00088-X](https://doi.org/10.1016/S0376-0421(02)00088-X)
- [15] O. Lucca-Negro and T. O'doherty, Vortex breakdown: a review. *Progress in Energy and Combustion Science*, 27 (4), 431–481, 2001. [https://doi.org/10.1016/S0360-1285\(00\)00022-8](https://doi.org/10.1016/S0360-1285(00)00022-8)
- [16] A. M. Mitchell and J. Détery, Research into vortex breakdown control. *Progress in Aerospace Sciences*, 37 (4), 385–418, 2001. [https://doi.org/10.1016/S0376-0421\(01\)00010-0](https://doi.org/10.1016/S0376-0421(01)00010-0)
- [17] Z.-Y. Lu and L.-G. Zhu, Study on forms of vortex breakdown over delta wing. *Chinese Journal of Aeronautics*, 17 (1), 13–16, 2004. [https://doi.org/10.1016/S1000-9361\(11\)60196-9](https://doi.org/10.1016/S1000-9361(11)60196-9)
- [18] G. E. Erickson, Water-tunnel studies of leading-edge vortices. *J. Aircr.* 19 (6): 442–448, 1982. <https://doi.org/10.2514/3.57414>
- [19] I. Gursul, Review of unsteady vortex flows over slender delta wings. *J. Aircr.* 42 (2): 299–319, 2005. <https://doi.org/10.2514/1.5269>
- [20] I. Gursul and Z. Wang, Flow control of tip/edge vortices. *AIAA Journal*, 56 (5), 1731-49, 2018. <https://doi.org/10.2514/1.J056586>
- [21] L. Shen, C.-Y. Wen, and H.-A. Chen, Asymmetric flow control on a delta wing with dielectric barrier discharge actuators. *AIAA Journal*, 54 (2), 652–8, 2016. <https://doi.org/10.2514/1.J054373>
- [22] M. Hadidoolabi and H. Ansarian, Computational investigation of vortex structure and breakdown over a delta wing at supersonic pitching maneuver. *Journal of the Brazilian Society of Mechanical Sciences and Engineering*, 40(2), 78, 2018. <https://doi.org/10.1007/s40430-018-1021-z>
- [23] N. M. Zain, S. Mat, K. A. Kasim, M. Shuhaimi, Md. Nizam Dahlan, N. Othman, Wind tunnel experiments on a generic sharp-edge delta wing UAV Model. *Journal of Advanced Research in Fluid Mechanics and Thermal Science*, 40 (1), 18-26, 2017.
- [24] M. Ozgoren, B. Sahin, and D. Rockwell, Vortex structure on a delta wing at high angle of attack. *AIAA*

- Journal, 40(2), 285-292, 2002. <https://doi.org/10.2514/2.1644>
- [25] A. Buzica, J. Bartasevicius, and C. Breitsamter, Experimental investigation of high-incidence delta-wing flow control. *Experiments in Fluids*, 58 (9), 131, 2017. <https://doi.org/10.1007/s00348-017-2408-9>
- [26] C. Cetin, A. Celik, and M. M. Yavuz, Control of flow structure over a nonslender delta wing using periodic blowing. *AIAA Journal*, 56 (1), 90–9, 2017. <https://doi.org/10.2514/1.J056099>
- [27] M. Zharfa, I. Ozturk, and M. M. Yavuz, Flow structure on nonslender delta wing: reynolds number dependence and flow control. *AIAA Journal*, 54 (3), 880–97, 2016. <https://doi.org/10.2514/1.J054495>
- [28] C. Canpolat, B. Sahin, S. Yayla, and H. Akilli, Effects of perturbation on the flow over nonslender delta wings. 45th AIAA Fluid Dynamics Conference, 2015. <https://doi.org/10.2514/6.2015-2307>
- [29] M. Ozgoren, Impingement of vortex breakdown upon an edge: flow structure and origin of loading. Ph. D. Thesis, Çukurova University Institute of Natural and Applied Sciences, Adana, 2000.
- [30] B. Yaniktepe and D. Rockwell, Flow structure on a delta wing of low sweep angle. *AIAA Journal*, 42 (3), 513–23, 2004. <https://doi.org/10.2514/1.1207>
- [31] S. P. Lemay, S. M. Batill, and R. C. Nelson, Vortex dynamics on a pitching delta wing. *Journal of Aircraft*, 27 (2), 131–38, 1990. <https://doi.org/10.2514/3.45908>
- [32] F. Gilliam, J. Wissler, J. Walker, and M. Robinson, Visualization of unsteady separated flow about a pitching delta wing. 25th AIAA Aerospace Sciences Meeting, 1987. <https://doi.org/10.2514/6.1987-240>
- [33] G. Reynolds and A. Abtahi, Instabilities in leading-edge vortex development. 5th Applied Aerodynamics Conference, USA, 1987.
- [34] I. Gursul and W. Xie, Buffeting flows over delta wings. *AIAA Journal*, 37, 58–65, 1999. <https://doi.org/10.2514/2.664>
- [35] S. Lemay, S. Batill, and R. Nelson, Leading edge vortex dynamics on a pitching delta wing. 6th Applied Aerodynamics Conference, USA, 1988.
- [36] D. S. Grismer and R. C. Nelson, Double-delta-wing aerodynamics for pitching motions with and without sideslip. *Journal of Aircraft*, 32 (6), 1303–11, 1995. <https://doi.org/10.2514/3.46879>
- [37] M. Ozgoren and B. Sahin, Effect of pitching delta wing on vortex structures with and without impingement plate. *Turkish J. Eng. Env. Sci*, 26, 325-43, 2002.

